Mon. Not. R. Astron. Soc. **303,** L47–L52 (1999)

Constraints on Ω_Λ and Ω_m from distant Type Ia supernovae and cosmic microwave background anisotropies

G. Efstathiou,[1] S. L. Bridle,[2] A. N. Lasenby,[2] M. P. Hobson[2] and R. S. Ellis[1]
[1] *Institute of Astronomy, Madingley Road, Cambridge CB3 0HA*
[2] *Cavendish Astrophysics Group, Cavendish Laboratory, Madingley Road, Cambridge CB3 0HE*

Accepted 1999 January 8. Received 1998 November 16

ABSTRACT

We perform a combined likelihood analysis of the latest cosmic microwave background anisotropy data and distant Type Ia supernova data of Perlmutter et al. Our analysis is restricted to cosmological models where structure forms from adiabatic initial fluctuations characterized by a power-law spectrum with negligible tensor component. Marginalizing over other parameters, our best-fitting solution gives $\Omega_m = 0.25^{+0.18}_{-0.12}$ and $\Omega_\Lambda = 0.63^{+0.17}_{-0.23}$ (95 per cent confidence errors) for the cosmic densities contributed by matter and a cosmological constant, respectively. The results therefore strongly favour a nearly spatially flat Universe with a non-zero cosmological constant.

Key words: cosmic microwave background – cosmology: miscellaneous.

1 INTRODUCTION

The aim of this paper is to constrain the geometry of the Universe by combining results from the cosmic microwave background (CMB) anisotropies with those from distant Type Ia supernovae. Recently, there have been a number of analyses of CMB anisotropies aimed at constraining cosmological parameters (Hancock et al. 1998; Bond & Jaffe 1997; Lineweaver & Barbosa 1998a,b; Webster et al. 1998). These papers show that the CMB already provides useful constraints on adiabatic inflationary models. The results described in this paper extend these analyses to a wider parameter set including closed Universes.

However, observations of CMB anisotropies alone cannot determine the geometry of the Universe unambiguously (Bond, Efstathiou & Tegmark 1997; Zaldarriaga, Spergel & Seljak 1997). This is because two models with identical fluctuation spectra and matter content will have nearly identical CMB power spectra if they have the same angular diameter distance to the last scattering surface. This *geometrical degeneracy* can be broken for extreme values of the cosmological parameters Ω_Λ and Ω_m by the inhomogeneous Sachs–Wolfe effect at low multipoles (see Efstathiou & Bond 1999), but for plausible parameters the degeneracy is nearly exact.[1]

A number of authors (White 1998; Tegmark et al. 1998; Efstathiou & Bond 1999) have shown that the magnitude–redshift relation for distant Type Ia supernovae (SN) provides nearly orthogonal constraints in the Ω_Λ–Ω_m plane to those derived from the CMB. The combination of CMB and SN data can thus provide tight constraints on the geometry of the Universe. This has been demonstrated by White (1998), Garnavich et al. (1998) and Lineweaver (1998) using the SN data of Perlmutter et al. (1997, 1998b) and Riess et al. (1998). In this paper, we use the larger sample of 42 high-redshift SN of Perlmutter et al. (1998a, hereafter P98, 1998b). The likelihood analysis of the CMB observations is described in Section 2. Section 3 describes the likelihood analysis of the SN data and the results from the combined data set are described in Sections 4 and 5.

[1] However, gravitational lensing of the CMB can break this degeneracy (see Seljak & Zaldarriaga 1998).

2 ANISOTROPIES OF THE COSMIC MICROWAVE BACKGROUND

The analysis presented here is similar to that described by Hancock et al. (1998) and we refer the reader to this paper for technical details. Similar analyses and compilations of observations are discussed by Lineweaver (1998, and references therein) and by Bond, Jaffe & Knox (1998). A window function W_l for each experiment is used to convert the observed level of anisotropy to flat bandpower estimates $(\Delta T_l/T) \pm \sigma$ centred on the effective multipole $l_{\rm eff}$ (defined as the half-power point of the window function). The resulting CMB data points are plotted in Fig. 1, together with their 68-per-cent confidence limits. These confidence limits have been obtained using likelihood analyses and hence incorporate uncertainties from random errors, sampling variance and cosmic variance.

The data points in Fig. 1 are identical to those given in Webster et al. (1998) except that we have added the three QMAP points (Ka and Q bands for flights 1 and 2, Devlin et al. 1998; Herbig et al. 1998; De Oliveira-Costa et al. 1998).

We fit the CMB data points to adiabatic CDM models specified by the following parameters: (1) amplitude Q_{10} of the $\ell = 10$ multipole defined as in Lineweaver (1998); (2) the density

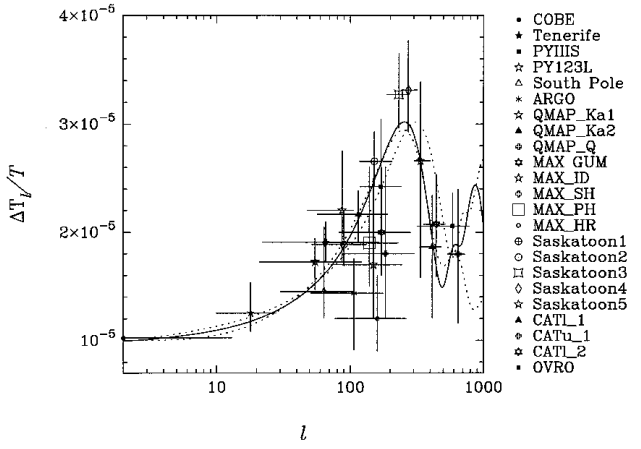

Figure 1. CMB bandpower anisotropy estimates for various experiments, as described in the text. The solid line shows the best-fitting adiabatic CDM model with parameters $Q_{10} = 1.14$, $n = 1.08$, $\omega_c = 0.36$, $\omega_b = 0.03$ and Doppler peak location parameter $\gamma_D = 1.18$. The dotted lines show the best-fitting curves with location parameter fixed at $\gamma_D = 0.8$ and $\gamma_D = 1.5$ (approximately the 2σ allowed range for γ_D).

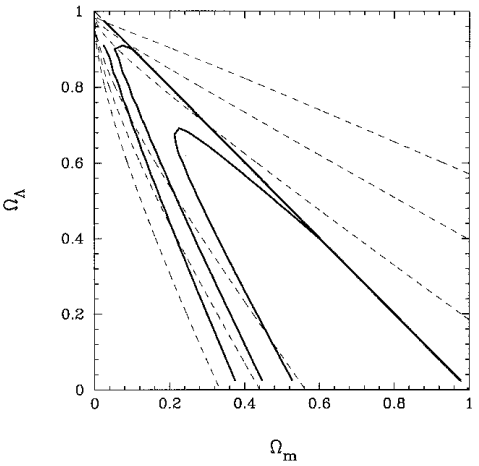

Figure 2. Likelihood contours in the Ω_Λ–Ω_m plane derived from the CMB data points shown in Fig. 1. The contours are plotted where $-2\ln\mathcal{L}/\mathcal{L}_{max}$ is equal to 2.29, 6.16 and 11.83, corresponding approximately to 1, 2 and 3σ confidence contours for a Gaussian likelihood function. The solid lines show the marginalized likelihood contours derived from the CMBFAST computations for $\omega_b = 0.019$. The dotted lines extending into the $\Omega_k < 0$ region show the equivalent contours derived from the fitting function approach described in the text. For the dotted contours, we have marginalized over ω_b, although this has very little effect.

parameters Ω_k and (3) Ω_Λ; (4) the scalar spectral index n_s; (5) the physical density in cold dark matter $\omega_c = \Omega_c h^2$;[2] (6) the physical density in baryons $\omega_b = \Omega_b h^2$. We ignore tensor modes in this analysis.[3]

The motivation for choosing this set of variables is explained in Efstathiou & Bond (1999, hereafter EB99). The physical densities ω_c and ω_b and the radiation density determine the sound speed at the time of recombination. The geometry of the universe is specified by the parameters Ω_k and Ω_Λ, and the Hubble constant enters as an auxiliary parameter

$$h = \left[\frac{(\omega_c + \omega_b)}{(1 - \Omega_k - \Omega_\Lambda)}\right]^{1/2}. \quad (1)$$

We have fitted the observations to the theoretical models using two methods. First, we compute a grid of theoretical power spectra in the parameters $\Omega_k, \Omega_\Lambda, n_s, \omega_c$, using the CMBFAST code of Seljak & Zaldarriaga (1996) with ω_b constrained to 0.019, the value inferred from primordial nucleosynthesis and the deuterium abundances measured from quasar spectra ($\omega_b = 0.019 \pm 0.001$, see Burles & Tytler 1998a,b). In its present form, the CMBFAST code is restricted to open and spatially flat models ($\Omega_k \geq 0$) and so we have adopted a second, approximate technique to extend the theoretical predictions to closed models. This is based on a semi-analytic fitting formula for the CMB power spectrum of $\Omega_k = 0$ models, which is a generalization of the fitting formula of equation (24) in EB99 and provides accurate fits to the first three Doppler peaks of the CMB power spectrum. The fitting formula includes the dependences on n_s, ω_b, ω_c and Ω_Λ, and is typically accurate to better than 5 per cent. For models with non-zero values of Ω_k, we use the scaling relation $C(\ell') \rightarrow C(\ell\gamma_D)$, where γ_D is a 'location' parameter,

$$\gamma_D \approx \frac{\ell_D(\Omega_k, \Omega_\Lambda)}{\ell_D(\Omega_k = 0, \Omega_\Lambda = 0)}, \quad (2)$$

where $\ell_D(\Omega_k, \Omega_\Lambda)$ is the location of the first Doppler peak given by equation (22) of EB99 generalized to models with $\Omega_k < 0$. The location parameter thus measures the positions of the Doppler peaks relative to those of a spatially flat model with zero cosmological constant. The approximate formula does not include the inhomogeneous Sachs–Wolfe effect (see e.g. Bond 1996), which affects low multipoles if Ω_k and Ω_Λ are non-zero. However, the inhomogeneous Sachs–Wolfe effect is a weak discriminator of cosmological models (see EB99) and, with the data shown in Fig. 1, the constraints on cosmological models are set primarily by the location of the first Doppler peak. A similar approximate technique, using rescaling of power spectra computed with CMBFAST, is described by Tegmark (1998).

Fig. 1 shows the best-fitting CMB power spectrum, together with the best-fitting curves with $\gamma_D = 0.8$ and 1.5 (spanning the 2σ-allowed range of γ_D after marginalization over other parameters). The present CMB data points evidently favour models with $\Omega_k \approx 0$. The large number of data points at $\ell \sim 100$ set quite strong constraints on closed models, but the lack of data points at $\ell \gtrsim 300$ leads to weaker constraints on open models. The CMB data do not yet allow strong constraints on the parameters ω_b and ω_c, hence the constraints on the Hubble constant (equation 1) are also extremely weak.

Fig. 2 shows the CMB constraints in the Ω_m–Ω_Λ plane. Here, we have marginalized over n_s, Q_{10}, ω_c (and ω_b for the likelihoods computed from the fitting formula) assuming uniform prior distributions in these parameters. The marginalized likelihood depends slightly on the range adopted for ω_c; in Fig. 2 we assume a uniform prior distribution over the range $0.05 \leq \omega_c \leq 0.5$. The marginalized likelihood function is insensitive to the ranges and prior distributions adopted for the other parameters and is insensitive to ω_b.

The results of this analysis are similar to those of Lineweaver (1998) and Tegmark (1998) but differ in detail. The main difference is in the way that we marginalize over the likelihood function. We have assumed a uniform prior distribution in each parameter and performed direct integrations over the full likelihood function.

[2] Here h is the Hubble constant in units of $100\,\mathrm{km\,s^{-1}\,Mpc^{-1}}$.

[3] For reasonable amplitudes of a tensor mode, the effect on the position of the first Doppler peak is small. A small tensor mode will therefore have little effect on the cosmological parameters Ω_Λ and Ω_m as these are determined primarily by the position of the first Doppler peak.

Lineweaver and Tegmark 'marginalize' over a subset of parameters by fixing them to their maximum likelihood values. Our approach provides more robust errors, although the marginalized likelihood function for poorly determined parameters will depend on the choice of prior (usually weakly). In the limit that the likelihood function is Gaussian, the two approaches are equivalent. However, for non-Gaussian likelihoods (as is the case with the present CMB data) the approach adopted by Lineweaver and Tegmark can give misleadingly small errors on some parameters.

3 MAGNITUDE–REDSHIFT RELATION FOR DISTANT SUPERNOVAE

We use the sample of 42 high redshift ($0.18 \leq z \leq 0.83$) supernovae of P98, supplemented with 18 low redshift ($z < 0.1$) Type Ia supernovae from the Calán/Tololo Supernova Survey (Hamuy et al. 1996). For each supernova, P98 computed a peak magnitude in the B band m_B, corrected for Galactic extinction and a 'stretch parameter' s that stretches the time axis of a template Type Ia lightcurve to match the observed lightcurve (see Perlmutter et al. 1995, 1997).

P98 provide a comprehensive analysis of the constraints on $\Omega_{\rm m}$ and Ω_Λ derived from the SN magnitude–redshift relation and of the effects of excluding various outlying SN, including or excluding corrections for the lightcurve width–luminosity relation, host galaxy extinction, etc. P98 show that the likelihood function in the $\Omega_{\rm m}$–Ω_Λ plane is remarkably stable to such changes. We do not repeat this analysis here, but instead concentrate on the analysis of the supernovae used in the 'primary fit' of P98 (their fit C), which excludes 4 high redshift objects. These are SN 1997O, 1996cg and 1996cn, which are very likely reddened by their host galaxies and so are fainter than the best-fitting magnitude–redshift relation, and SN 1994H, which is not spectroscopically confirmed as a Type Ia SN and lies brighter than the best-fitting relation. In agreement with the results of P98, none of our conclusions change significantly if we include these supernovae.

We define a corrected peak magnitude $m_B^{\rm corr}$ for the lightcurve width–luminosity effect

$$m_B^{\rm corr} = m_B + \alpha\,(s-1), \tag{3}$$

where s is the measured stretch factor and α is a constant to be determined. These corrected magnitudes are compared with the predicted magnitudes

$$m_B^{\rm pred}(z) = \mathcal{M}_B + 5\log \mathcal{D}_L(z,\Omega_{\rm m},\Omega_\Lambda), \tag{4}$$

where $\mathcal{M}_B$ is related to the corrected absolute magnitude M_B by $\mathcal{M}_B = M_B - 5\log H_0 + 25$, and $\mathcal{D}_{\rm L} = d_{\rm L} + 5\log H_0$ is the Hubble-constant-free luminosity distance defined by P98. To compute the luminosity distance, we ignore gravitational lensing and use the standard expression for a universe with uniform density (see e.g. Peebles 1993),

$$d_{\rm L}(z,\Omega_{\rm m},\Omega_\Lambda) = \frac{c}{H_0}\frac{(1+z)}{|\Omega_{\rm k}|^{1/2}}\,{\rm sin_k}\left[|\Omega_{\rm k}|^{1/2}x(z,\Omega_{\rm m},\Omega_\Lambda)\right],$$
$$x(z,\Omega_{\rm m},\Omega_\Lambda) = \int_0^z \frac{{\rm d}z'}{[\Omega_{\rm m}(1+z')^3+\Omega_{\rm k}(1+z')^2+\Omega_\Lambda]^{1/2}}, \tag{5}$$

where $\Omega_{\rm k} = 1-\Omega_{\rm m}-\Omega_\Lambda$ and $\sin_{\rm k} = \sinh$ if $\Omega_{\rm k} > 0$ and $\sin_{\rm k} = \sin$ for $\Omega_{\rm k} < 0$. We assume a constant cosmological constant here rather than an arbitrary equation of state as might arise with scalar fields that become important at late times (Ratra & Peebles 1988; Caldwell, Dave & Steinhardt 1998). The biases in the magnitude–redshift relation arising from gravitational lensing should be negligible for CDM-like models unless a large fraction of the dark matter is in compact objects (e.g. Wambsganss, Cen & Ostriker 1998). Even in the latter case, P98 show that the biases are relatively small for the low matter densities favoured by the SN data.

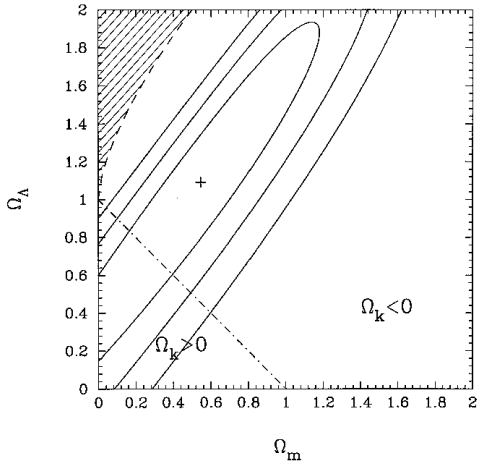

Figure 3. Likelihood contours (1, 2 and 3σ, as defined in the caption to Fig. 2) in the Ω_Λ–$\Omega_{\rm m}$ plane derived from the SN magnitude–redshift relation after marginalization over the parameters $\mathcal{M}_B$ and α. The cross shows the maximum likelihood solution. Bouncing universes have parameters within the hatched region.

With the above assumptions, we perform a four-parameter ($\Omega_{\rm m}$, Ω_Λ, $\mathcal{M}_B$ and α) likelihood analysis assuming Gaussian errors on $m_B^{\rm corr}$ consisting of three terms,

$$(\Delta m_B^{\rm corr})^2 = \Delta m_B^2 + \alpha^2\Delta s^2 + \Delta m_{\rm intrinsic}^2, \tag{6}$$

where Δm_B and Δs are the measurement errors in m_B and s and $\Delta m_{\rm intrinsic}$ is the instrinsic dispersion in m_B determined to be 0.18 mag from the Calán/Tololo sample. (The maximimum likelihood parameters are extremely insensitive to $\Delta m_{\rm intrinsic}$.) This analysis differs from that in P98 in that we include the dependence of the magnitude errors on the parameter α self-consistently in the likelihood analysis via equation (6). As we will see below this has little effect on the likelihood constraints on Ω_Λ and $\Omega_{\rm m}$ (Fig. 3), which are in good agreement with the results presented in P98. However, our analysis allows an important test of the intrinsic properties of high and low redshift supernovae (see Fig. 4).

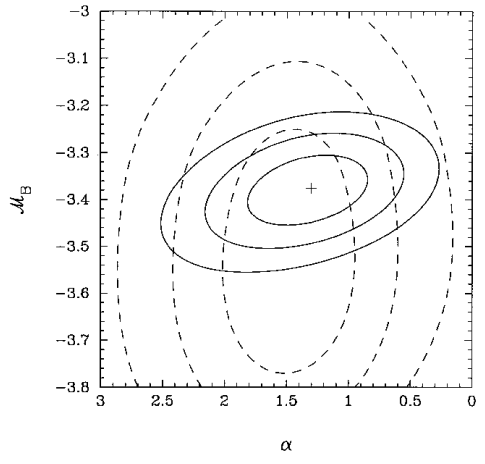

Figure 4. Likelihood contours (1, 2 and 3σ) in the $\mathcal{M}_B$–α plane. The solid lines show contours for the Calán/Tololo sample and the dotted lines show contours for the high redshift P98 sample after marginalization over the cosmological parameters Ω_Λ and $\Omega_{\rm m}$.

Table 1. Maximum likelihood parameters.

$\mathcal{M}_B$	α	$\Omega_{\rm m}$	Ω_Λ	Sample
−3.45	1.33	0.54	1.09	combined
−3.69	1.41	0.75	1.86	high z
−3.37	1.32	–	–	low z

Excluding the four SN as described above, we analyse the combined high redshift P98 + Calán/Tololo samples (denoted 'combined'), and the two samples separately (denoted 'high z' and 'low z', respectively). The magnitude–redshift relation of the low-z sample is relatively insensitive to cosmology, hence we fix $\Omega_{\rm m} = 1$ and $\Omega_\Lambda = 0$ in the likelihood analysis. Table 1 lists the parameters that maximize the likelihood for these samples.

Fig. 3 shows the likelihood function for the combined sample in the Ω_m–Ω_Λ plane after marginalization over the parameters $\mathcal{M}_B$ and α assuming uniform prior distributions in these variables. We use this likelihood function in Section 3 when we combine the SN sample with parameters derived from the CMB. As P98 show (and we have confirmed) changes in the analysis, e.g. omitting outliers, stretch correction, reddened objects, usually shifts the error ellipses by much less than the width of the 1σ contour.

An important consistency check is the agreement between the intrinsic properties of the high and low redshift SN. This is illustrated in Fig. 4, which shows likelihood contours for the parameters $\mathcal{M}_B$ and α for the low-z and high-z samples (marginalized over Ω_Λ and $\Omega_{\rm m}$ for the high-z sample). This diagram shows that the low-z and high-z samples have the same lightcurve width–luminosity relation and consistent peak absolute magnitudes $\mathcal{M}_B$. (Note, however, that the contours for the high-z sample become highly elongated in the $\mathcal{M}_B$ direction because this parameter correlates strongly with Ω_Λ and $\Omega_{\rm m}$). We have repeated the likelihood analysis including the intrinsic magnitude scatter $\Delta m_{\rm intrinsic}$ as a free parameter. For the low-z sample, the likelihood gives a broad distribution peaked at $\Delta m_{\rm intrinsic} = 0.18$, consistent with the rms residual of 0.16 mag of the Calán/Tololo points around the best-fitting solution. The combined sample gives $\Delta m_{\rm intrinsic} = 0.20$, slightly higher but consistent with the low-z sample. (In fact, $\Delta m_{\rm intrinsic}$ drops to 0.18 mag if we remove three outliers, SN92bi, SN95as and SN97K.)

For low redshift supernovae, the lightcurve widths and luminosities are known to correlate with the morphological type of the host galaxies (Hamuy et al. 1996). Thus the lack of any significant difference between the high and low redshift samples in Fig. 2 provides a constraint on evolutionary corrections associated with systematic changes in the host galaxies with redshift (e.g. metallicity, morphological mix). Fig. 4 therefore indicates no detectable evolutionary trends in the underlying supernova population used in this analysis.

Table 1 shows that the high-z sample alone yields values for $\Omega_{\rm m}$ and Ω_Λ that are similar to those of the combined sample. However, the error contours for the high-z sample are much larger than those shown in Fig. 1 for the combined sample so that a $\Omega_{\rm m} = 1$, $\Omega_\Lambda = 0$ universe lies within the 2σ contour. The narrowness of the likelihood contours shown in Fig. 3 therefore rely on combining the P98 data with the Calán/Tololo sample, although the general trends are evident in the high-z sample alone.

In summary, the P98 and Calán/Tololo SN strongly favour a universe with $0.78\Omega_{\rm m} - 0.62\Omega_\Lambda \approx -0.25 \pm 0.13$. This is consistent with the analysis of P98 (who find $0.8\,\Omega_{\rm m} - 0.6\,\Omega_\Lambda \approx -0.2 \pm 0.1$) and with the analysis of a sample of 16 SN at $z > 0.16$ (14 of which are independent of the P98 high redshift sample) combined with 34 low-z SN from the Calán/Tololo and CfA samples (Riess et al. 1998; Garnavich et al. 1998). Furthermore, the lightcurve width–luminosity relation of the high-z SN is consistent with that of the nearby sample suggesting that these objects have similar intrinsic properties. If an evolutionary effect is causing a systematic error in the magnitude–redshift relation of the distant sample, then it must be so as to preserve the lightcurve width–luminosity relation.

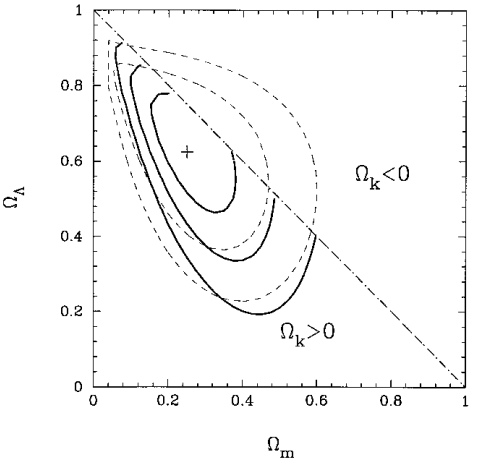

Figure 5. Likelihood contours derived by combining the supernovae likelihood function shown in Fig. 3 with the CMB likelihood function shown in Fig. 2. As in Fig. 2, solid contours show 1, 2 and 3σ confidence intervals computed using CMBFAST. The dashed contours show 2 and 3σ contours computed using the approximate CMB fitting technique (for clarity we do not plot the 1σ contour). The combined CMB+SN likelihood function peaks at $\Omega_{\rm m} = 0.25$ and $\Omega_\Lambda = 0.63$.

4 COMBINING THE SUPERNOVAE AND CMB LIKELIHOODS

4.1 Combined likelihoods

The combined likelihood obtained by multiplying the SN and CMB likelihoods are shown in Fig. 5. As in Fig. 2, the solid lines show the likelihood computed with CMBFAST and the dashed lines show the approximate technique indicating how the contours extend into the $\Omega_{\rm k} < 0$ regime. The likelihood peaks at $\Omega_{\rm m} = 0.25$ and $\Omega_\Lambda = 0.63$. The combined likelihood thus strongly favours a nearly spatially flat Universe with a low matter density and high cosmological constant. In fact, the 2σ ellipse in Fig. 5 extends over the range $\Omega_{\rm m} \approx 0.12$, $\Omega_\Lambda = 0.84$, to $\Omega_{\rm m} \approx 0.49$ and $\Omega_\Lambda = 0.51$. A high value of Ω_Λ is suggested by the SN data alone, and is required if we impose the constraint $\Omega_{\rm k} = 0$ (see fig. 7 of P98; fig. 6 Riess et al. 1998). However, from the SN data alone we cannot rule out an open Universe with a low matter density $\Omega_{\rm m} \lesssim 0.1$ and zero cosmological constant. Since the CMB data favour a universe with $\Omega_{\rm k} = 0$, the combined SN+CMB data *require a non-zero cosmological constant at a high significance level*. This is the main result of this paper.

Fig. 6 provides another illustration of how the combination of CMB and SN data dramatically improve the constraints on Ω_Λ and Ω_m. Here we have plotted the likelihood functions marginalized over all other parameters except $\Omega_{\rm m}$ (Fig. 6a) and Ω_Λ (Fig. 6b) for the SN and CMB data alone and for the combined data sets. For a Gaussian likelihood function, the 95-per-cent confidence region is delineated by $\mathcal{L}/\mathcal{L}_{\rm max} \geq 0.146$ and so we can see from Fig. 6 that the constraints on Ω_m and Ω_Λ from the SN and CMB data alone are extremely weak. However, for the combined data sets we find

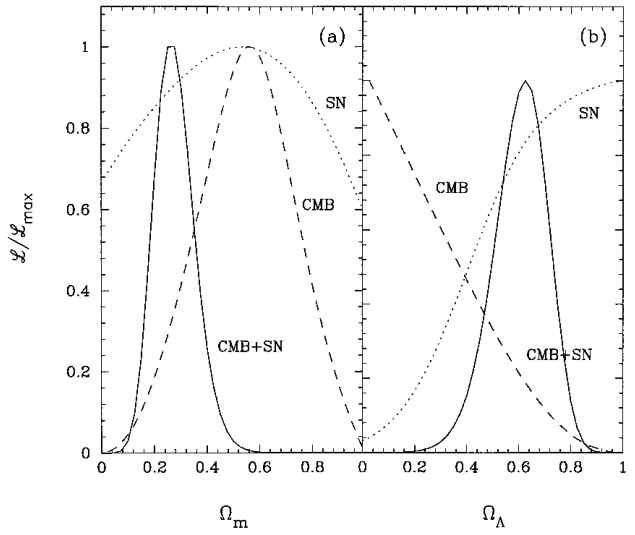

Figure 6. Marginalized likelihood functions plotted as function of Ω_m (left-hand panel) and Ω_Λ (right-hand panel). The dotted lines are for the SN data alone (Fig. 3), dashed lines for the CMB data alone (Fig. 2) and solid lines for the combined data sets (Fig. 5).

$\Omega_m = 0.25^{+0.18}_{-0.12}$ and $\Omega_\Lambda = 0.63^{+0.17}_{-0.23}$ at the 95-per-cent confidence level.

4.2 Systematic errors

Systematic errors in the analysis of the SN data are discussed at length by P98 and Riess et al. (1998). No systematic error has yet been identified that could produce a large downward shift of the SN likelihood contours in Fig. 3. Possible sources of systematic error include differences in the reddening caused by the host galaxies, and evolutionary (e.g. metallicity dependent) corrections to the SN absolute magnitude–redshift relation. Internal reddening for this sample is discussed in detail by P98. They find no excess reddening of most of the distant SN when compared with the Calán/Tololo sample, although there are a small number of possibly reddened SN (three of which have been excluded in this analysis). The inclusion or exclusion of these reddened objects does not significantly affect Fig. 5. Grey extinction is much harder to rule out, but may not be physically well motivated.

Possible evolutionary effects are difficult to check. However, the results summarized in Fig. 4 show that the high and low redshift SN sample have statistically indistinguishable internal properties, i.e. they have consistent lightcurve width–luminosity relations and (within rather large errors) consistent peak absolute magnitudes $\mathcal{M}_B$. With a larger sample of SN it should be possible to refine this test and to test for differences in the distribution of lightcurve shapes with redshift. Another consistency check would be provided by extending the SN sample to $z > 1$. As Goobar & Perlmutter (1995) have discussed, the degeneracy of the magnitude–redshift relation in the Ω_m–Ω_Λ plane can be broken by a sample of SN spanning a sufficiently wide range of redshifts.

4.3 The best-fitting Universe

If systematic errors are indeed small, the combined CMB and SN data strongly favour a nearly spatially flat Universe with $\Omega_m \approx 0.25$ and $\Omega_\Lambda \approx 0.63$. These values are close to those favoured by a number of other arguments, which we summarize briefly below (see also e.g. Ostriker & Steinhardt 1995, P98, and references therein).

Age and Hubble constant

For our best-fitting cosmology, the age of the Universe is $14.6(h/0.65)^{-1}$ Gyr (in agreement with P97). This is compatible with recent estimates of 11.5 ± 1.3 Gyr for the ages of the oldest globular clusters (see Chaboyer 1998) and with recent values of H_0 derived from Type Ia supernovae and Cepheid distances, which fall within the range $H_0 = 65 \pm 10\,\mathrm{km\,s^{-1}Mpc^{-1}}$ (e.g. Freedman et al. 1998).

Large-scale structure

Observations of large-scale structure (see e.g. Efstathiou 1996 for a review) are consistent with scale-invariant adiabatic cold dark matter universes if $\Gamma \approx \Omega_m h \approx 0.2$–$0.3$. This is broadly consistent with the analysis presented here and with the analysis of combined CMB and IRAS galaxy data presented by Webster et al. (1998).

Baryon abundance in clusters

Consistency between primordial nucleosynthesis ($\omega_b \approx 0.019$) and the ratio of baryons in clusters to total cluster mass ($f_b \approx 0.06h^{-3/2}$, see Evrard 1997 and references therein) requires a low matter density, $\Omega_m \approx 0.26(h/0.65)^{-1/2}$, consistent with the best-fitting solution of Fig. 5.

5 CONCLUSIONS

(i) We have applied an approximate formula for the CMB power spectrum that can be used to constrain a wide set of cosmological parameters, including closed universes, by fitting to the CMB anisotropy data. The results agree well with those derived from exact computations using the CMBFAST code.

(ii) In our analysis we perform a proper marginalization over parameters, assuming uniform prior distributions, to derive constraints in the Ω_m–Ω_Λ plane and on Ω_m and Ω_Λ separately.

(iii) Current CMB anisotropy data provide strong constraints on the position of the first Doppler peak and favour a spatially flat Universe.

(iv) A likelihood analysis of the SN data provides robust constraints on Ω_m and Ω_Λ consistent with those derived by P98. For a spatially flat Universe, the SN data require a non-zero cosmological constant at a high level of significance ($\Omega_\Lambda \gtrsim 0.5$ at 95-per-cent confidence).

(v) The lightcurve width–luminosity relation for high redshift and low redshift SN are statistically indistinguishable, consistent with no evolution of the SN population.

(vi) The combination of CMB and SN data thus provides strong constraints on Ω_m and Ω_Λ favouring values of $\Omega_m \approx 0.25$ and $\Omega_\Lambda \approx 0.63$. If there are no significant systematic effects in the SN data (e.g. grey dust, evolution) then we are forced into accepting a cosmological constant or a 'quintessence-like' component of the Universe (Caldwell et al. 1998; Garnavich et al. 1998).

(vii) There are a number of independent lines of argument, e.g. the age of the Universe, large-scale clustering of galaxies and the baryon content of clusters, to support the best-fitting parameters derived in this paper.

ACKNOWLEDGMENTS

G. Efstathiou thanks PPARC for the award of a Senior Fellowship. S. Bridle acknowledges the receipt of a PPARC studentship. We thank the members of the Supernova Cosmology Project for allowing us to use their data, especially Saul Perlmutter, who provided many helpful comments on this manuscript, and also Mike Irwin and Gerson Goldhaber for discussions of the P98 analysis. We thank Graca Rocha for assistance in preparing the CMB data points.

REFERENCES

Bond J. R., 1996, in Schaeffer R., Silk J., Spiro M., Zinn-Justin J., eds, Cosmology and Large Scale Structure. Elsevier Science, Amsterdam, p. 469

Bond J. R., Jaffe A., 1997, in Bouchet F., ed., Proc. XVIth Moriond Astrophysics meeting. Edition Frontières, Gif-Sur-Yvette, p. 197

Bond J. R., Efstathiou G., Tegmark M., 1997, MNRAS, 291 L33

Bond J. R., Jaffe A. H., Knox L. E., 1998, preprint (astro-ph/9808264)

Burles S., Tytler D., 1998a, in Mezzacappa A., ed., Proc. Second Oak Ridge Symp. on Atomic & Nuclear Astrophysics. Institute of Physics, Bristol (astro-ph/9803071)

Burles S., Tytler D., 1998b, ApJ, 507, 732

Caldwell R. R., Dave R., Steinhardt P. J., 1998, Phys Rev. Lett., 80, 1582

Chaboyer B., 1998, Phys. Rep., in press (astro-ph/9808200)

Devlin M. J., De Oliveira-Costa A., Herbig T., Miller A. D., Netterfield C. B., Page L., Tegmark M., 1998, ApJ, 509, L69

De Oliveira-Costa A., Devlin M. J., Herbig T., Miller A. D., Netterfield C. B., Page L., Tegmark M., 1998, ApJ, 509, L77

Efstathiou G., 1996, in Schaeffer R., Silk J., Spiro M., Zinn-Justin J., eds, Cosmology and Large Scale Structure. Elsevier Science, Amsterdam, p. 135

Efstathiou G., Bond J. R., 1999, MNRAS, in press (astro-ph/9807130) (EB99)

Evrard G., 1997, MNRAS, 292, 289

Freedman J. B., Mould J. R., Kennicutt R. C., Madore B. F., 1998, in IAU Symp. 183. Kluwer, Dordrecht, in press (astro-ph/9801090)

Garnavich P. M. et al. 1998, ApJ, 509, 74

Goobar A., Perlmutter S., 1995, ApJ, 450, 14

Hamuy M., Phillips M. M., Maza J., Suntzeff N. B., Schommer R. A., Aviles R., 1996, AJ, 112, 2391

Hancock S., Rocha G., Lasenby A. N., Gutierrez C. M., 1998, MNRAS, 294, L1

Herbig T., De Oliveira-Costa A., Devlin M. J., Miller A. D., Page L., Tegmark M., 1998, ApJ. 509, L73

Lineweaver C. H., 1998, ApJ, 505, L69

Lineweaver C. H., Barbosa D., 1998a, ApJ, 446, 624

Lineweaver C. H., Barbosa D., 1998b, A&A, 329, 799

Ostriker J. P., Steinhardt P. J., 1995, Nat, 377, 600

Peebles P. J. E., 1993, Principles of Physical Cosmology. Princeton University Press, Princeton, NJ

Perlmutter S. et al., 1995, in Presentations at the NATO ASI in Aiguablava, Spain, LBL-38400; also published 1997, in Ruiz-Lapuente P., Cana R., Isern J., eds, Thermonuclear Supernova. Dordrecht, Kluwer, p. 749

Perlmutter S. et al., 1997, ApJ, 483, 565

Perlmutter S. et al., 1998a, ApJ, in press (astro-ph/9812133) (P98)

Perlmutter S. et al., 1998b, in Presentation at the January 1988 Meeting of the American Astronomical Society, Washington DC, LBL-42230 (www-supernova.lbl.gov); 1997, BAAS, 29, 1351

Perlmutter S. et al., 1998c, Nat, 391, 51

Ratra B., Peebles P. J. E., 1988, Phys. Rev. D 37, 3406

Riess A. et al., 1998, AJ, 116, 1009

Seljak U., Zaldarriaga M., 1996, ApJ, 469, 437

Seljak U., Zaldarriaga M., 1998 (astro-ph/9811123)

Tegmark M., 1997, Phys. Rev. Lett., 79, 3806

Tegmark M., 1998, ApJL, submitted (astro-ph/9809201)

Tegmark M., Eisenstein D. J., Hu W., Kron R. G., 1998 (astro-ph/9805117)

Wambsganss J., Cen R., Ostriker J. P., 1998, ApJ, 494, 29

Webster M., Bridle S. L., Hobson M. P., Lasenby A. N., Lahav O., Rocha G., 1998, ApJL, 509, L65

White M., 1998, ApJ, 506, 495

Zaldarriaga M., Spergel D. N., Seljak U., 1997, ApJ, 488, 1

This paper has been typeset from a $\TeX/\LaTeX$ file prepared by the author.